# Proof-of-Concept Validation in Healthy Participants of an sEMG-Controlled 4-DOF Upper Limb Exoskeleton for Post-Stroke Rehabilitation

ANG LING WEAY* AND TANG MING

*School of Artificial Intelligence and Computing, Malaysia University of Science and Technology (MUST), Block B, Encorp Strand Garden Office, 12, Jalan PJU 5/5, Kota Damansara, 47810 Petaling Jaya, Selangor, Malaysia*

**Corresponding author: ang.weay@must.edu.my*

*(Received: 7 July 2026; Accepted: 2 September 2026; Published online: 11 September 2026)*

***ABSTRACT:*** Two improvements are needed in upper-limb exoskeletons (ULEs) for rehabilitation after stroke: a mechanism for the shoulder joint that will ensure interaction forces are minimized throughout the entire joint's range of motion and an easy-to-use interface that detects neural intent. These have previously been addressed separately; here, we validate them together in one integrated device, the first closed-loop 4-DOF ULE with a surface electromyography (sEMG)-based classification interface. The objective is to test, in healthy participants, whether an anatomically aligned shoulder mechanism preserves sEMG signal quality during physical coupling while a lightweight classifier recognizes movement intent in real time. The mechanism uses three revolute glenohumeral joints whose axes intersect at the shoulder center of rotation (COR), giving the basic shoulder degrees of freedom (DOF) with minimal acromion interference, plus a proximal joint emulating the sternoclavicular joint to expand the workspace; an elbow joint completes the kinematic chain. The controller identifies four activities of daily living (ADL), namely shoulder abduction (SAB), pick-up cup (PUC), push-forward cup (PFC), and rest arm (RA). These activities are recognized by classifying a 72-dimensional feature vector (6 features × 12 channels) at 16 Hz, using a 125 ms sliding time window and a linear support vector machine (SVM). In a closed-loop study with 15 healthy volunteers, recognition accuracy was 92.4%, 89.7%, and 85.1% for SVM, artificial neural network (ANN), and logistic regression, respectively; SVM recall was 96% (SAB) and 98% (RA). End-to-end latency was 148 ± 19 ms, below the accepted 200 ms threshold. Participants rated the system "Good" (SUS 71.3 ± 8.4) with only slight discomfort (NRS 1.8 ± 0.7). Misclassification was dominated by the kinematically adjacent PUC–PFC pair. As validation used healthy participants, these findings establish technical feasibility as a precursor to future clinical trials in stroke patients.

***ABSTRAK:*** Eksoskeleton anggota atas (upper limb exoskeletons, ULE) untuk pemulihan pasca-strok memerlukan dua kemajuan: mekanisme bahu yang mengekalkan daya interaksi rendah sepanjang julat pergerakan, dan antara muka intuitif yang mengecam niat neuro-otot tanpa beban mental tambahan. Kedua-duanya sebelum ini ditangani secara berasingan; di sini kami mengesahkan gabungannya dalam satu peranti bersepadu — ULE 4-DOF gelung tertutup pertama dengan antara muka pengelasan sEMG. Objektif kajian ialah menguji, dengan peserta sihat, sama ada mekanisme bahu yang sejajar secara anatomi dapat mengekalkan kualiti isyarat sEMG semasa gandingan fizikal, sementara pengelas ringan mengecam niat pergerakan secara masa nyata. Mekanisme ini menggunakan tiga sendi glenohumeral berputar yang paksinya bersilang pada pusat putaran (center of rotation, COR) bahu dengan gangguan minimum pada akromion, serta satu sendi proksimal yang meniru sendi sternoklavikular untuk memperluas ruang kerja; satu sendi siku melengkapkan rantaian kinematik. Pengawal tersebut mengenal pasti empat jenis aktiviti kehidupan harian (Activities

https://doi.org/10.31436/iiumej.v27i3.4578

of Daily Living, ADL), iaitu abduksi bahu (Shoulder Abduction, SAB), mengambil cawan (Pick-Up Cup, PUC), menolak cawan ke hadapan (Push Forward Cup, PFC), dan merehatkan lengan (Rest Arm, RA). Aktiviti-aktiviti ini dikelaskan melalui vektor ciri berdimensi 72 (6 ciri × 12 saluran) pada kadar 16 Hz, menggunakan tetingkap masa gelongsor 125 ms dan Mesin Vektor Sokongan linear (linear SVM). Dalam eksperimen gelung tertutup dengan 15 subjek sihat, ketepatan pengecaman ialah 92.4%, 89.7%, dan 85.1% masing-masing bagi SVM, rangkaian neural buatan (ANN), dan regresi logistik; kepekaan (recall) SVM ialah 96% (SAB) dan 98% (RA). Kependaman hujung-ke-hujung ialah 148 ± 19 ms, di bawah ambang 200 ms yang boleh diterima. Peserta menilai sistem ini "Baik" (SUS 71.3 ± 8.4) dengan sedikit ketidakselesaan sahaja (NRS 1.8 ± 0.7). Salah pengelasan didominasi oleh pasangan PUC–PFC yang berdekatan secara kinematik. Oleh kerana pengesahan dijalankan ke atas peserta sihat, dapatan ini merupakan langkah awal kepada ujian klinikal dengan pesakit strok.

***KEYWORDS:*** *Upper Limb Exoskeleton, sEMG Pattern Recognition, Rehabilitation Robotics, 4-DOF Shoulder Mechanism, Closed-Loop Control.*

## 1. INTRODUCTION

Stroke is the second leading global cause of death and third leading cause of disability, leaving more than 70% of survivors with chronic upper limb hemiparesis [1]. Restoration of upper limb function is the primary goal of post-acute rehabilitation, yet the intensive, high-dosage training required to drive neuroplasticity is difficult to deliver consistently through manual therapy alone due to clinician shortages and therapist fatigue [2, 3]. Robotic-assisted upper limb exoskeletons (ULEs) offer high-repetition movement assistance that can be delivered, quantified, and adapted to individualized motor intentions [3].

Adoption for clinical use is restricted by the mechanical problems that persist. In the shoulder complex, there is a complicated structure, and the movement of several joints results in translation of the COR of the glenohumeral joint [3]. Exoskeletons that constrain motion to a fixed mechanical pivot generate parasitic interaction forces that lead to shear, localized pressure, and compensatory movements, ultimately resulting in device rejection or joint damage [4, 5]. Traditional configurations are also susceptible to kinematic singularities and potential collisions with the operator's head or body as a result of complex motion tasks [5]. By designing redundant kinematic chains like 4-DOF active configurations and redundant 2R-3R-2R configurations, collision-free zones could be created and the workspace would be expanded to more closely approximate biological reachability [4].

The second problem is non-intuitive control, as most current platforms drive the upper-limb exoskeleton (ULE) along pre-programmed trajectories triggered by button presses or simple amplitude-threshold signals [6, 7]. This approach positions the patient as a passive recipient of movement rather than an active agent, which is contrary to modern neurorehabilitation theory [7]. Active volitional engagement is a prerequisite for cortical reorganization and durable functional recovery: actively generated movement produces greater performance gains and more pronounced motor-cortical reorganization than passive movement matched for kinematics [8], so the patient must intentionally initiate movement in order to drive neuroplasticity [2, 3]. Surface electromyography (sEMG) pattern recognition—the classification of spatial and temporal muscle activation into discrete intent classes—was established as a viable multifunction control strategy in the prosthetics literature [9], [10] and has since been proposed as the key enabling technology for achieving active, intent-driven rehabilitation control [3, 6].

Though both mechanical design and classifiers have been studied separately, the two have not yet been validated together as part of a single system [3, 6]. Classifiers have been evaluated based on signal obtained without any form of physical connection, whereas the design of the shoulder mechanisms has often lacked a proper intent-recognition pipeline [4, 11]. This is a critical issue, as physical connection introduces vibration and joint loading effects as well as perturbation of the electrode contacts which could affect the sEMG signal quality and thus the classification performance [4, 11]. On the other hand, the alignment of the kinematics would determine how large the perturbations could become due to the misalignment causing unnecessary interaction forces and hence the compensatory motions and rejection of the devices [3-5].

In this paper, we will be presenting a closed-loop validation of three systems – a four degree of freedom mechanical shoulder mechanism, real-time sEMG pipeline and the pattern recognition classifier – together as a single system. The validation is conducted in healthy participants as a proof-of-concept precursor to trials in stroke patients; clinical validation in the target population remains future work [4, 6].

This paper makes three scientific contributions, each addressing a distinct aspect of the integrated validation. First, the contribution to validating the mechanical design: we experimentally verify, on participants physically wearing the device, that the anatomically aligned 4-DOF shoulder mechanism supports functional activities of daily living while keeping compensatory movement low [3, 4]. Second, the contribution to validating the sEMG intent-recognition system: we quantify online, closed-loop classification accuracy and end-to-end latency for four daily-living movement classes under real device use, together with participant-reported usability and comfort [5, 6]. Third, the contribution to demonstrating the interaction between both systems through physical coupling: by comparing signal-to-noise ratio with and without device coupling on the same participants, we quantify how the mechanical design affects sEMG signal quality, and we frame this within a structured comparison of pattern-recognition versus proportional control [4, 6].

## 2. BACKGROUND AND FRAMING

### 2.1. The Glenohumeral Misalignment Problem

As shown in Fig. 1, the human shoulder complex involves four articulations that move in a coordinated fashion during arm elevation [2, 3]. The glenohumeral (GH) joint provides the dominant 3-DOF rotational motion, but its center of rotation (COR) is not stationary in the thoracic frame; specifically, the humeral head migrates dynamically during abduction as it must clear the acromion process [4]. Recent biomechanical research confirms that this translation—which can involve displacements of approximately 10 mm is essential for achieving a full range of motion [5]. The ball joint used as an exoskeleton joint does not provide a possibility for such translation and always causes kinematic incompatibility and the appearance of parasitic forces causing shear, localization of loads, and compensatory actions [4, 5]. Such interaction forces increase as the angle of abduction grows, and can cause rejection of the device or injuries to the joints themselves [4, 5].

Conventional 3R shoulder configurations, in which three revolute joints are connected in series to approximate the 3-DOF glenohumeral articulation, offer advantages in simplicity and control but suffer from three fundamental limitations (Fig. 2(a)). First, a singularity occurs when the arm reaches vertical elevation, causing the abduction and internal/external rotation axes to align and rendering independent rotation impossible. Second, the physical bulk of motors and linkages above and behind the shoulder creates collision risk with the user's head and torso at abduction angles beyond approximately 90°, severely restricting the usable workspace. Third, even modified 3R designs with a tilted base axis (Fig. 2(b)) — which improve the abduction range — cannot resolve the singularity problem or provide the scapular mobility needed for cross-body and overhead movements.

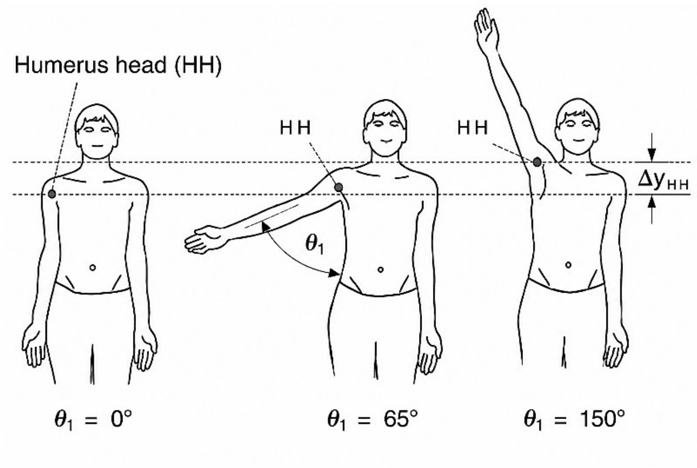


**Figure 1**. Location of the humeral head at different arm abduction angles in the frontal plane

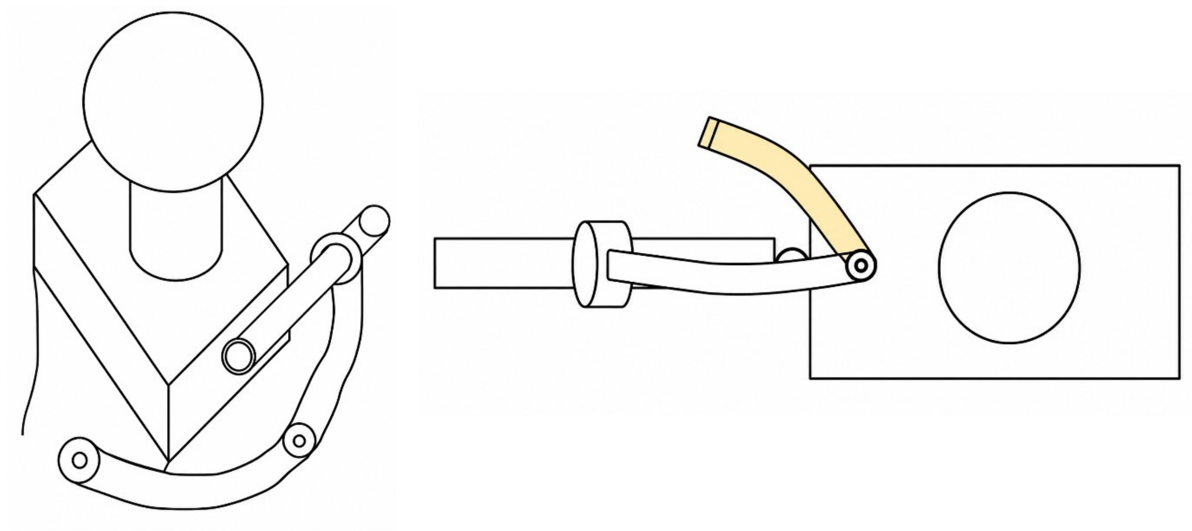

(a) (b)

**Figure 2**. Comparison of serial 3R shoulder configurations: (a) conventional configuration and (b) modified configuration with a tilted base axis.

## 2.2. The 4R Redundant Shoulder Configuration

Adding a fourth revolute joint to create a 4R configuration introduces kinematic redundancy: the mechanism has more DOFs than are strictly required to position and orient the upper arm, providing multiple joint-configuration paths to the same end-effector pose. This redundancy can be exploited to continuously avoid singularities and to navigate around collision obstacles by selecting configurations that maintain safe clearance from the user's head and torso (Fig. 3). The fourth joint in the present design is placed proximally to replicate the protraction/retraction and elevation/depression of the sternoclavicular joint and scapular girdle, which is the primary mechanism by which the shoulder complex expands its reach for cross-body, overhead, and backward extension movements.

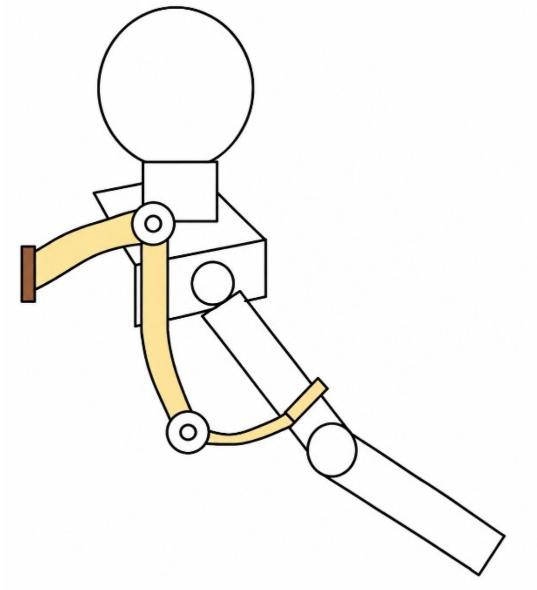

**Figure 3**. Four-revolute-joint (4R) redundant shoulder configuration.

### 2.3. Pattern Recognition vs. Proportional Control for Rehabilitation

In proportional myoelectric control, the amplitude envelope of the sEMG signal is mapped directly to a joint torque or velocity command, and it remains the most commonly used approach in commercial myoelectric controllers and EMG-driven rehabilitation robots [7, 11]. Although this characteristic (i.e., continuous modulation of the command through continuous muscle activation) was its main defining feature, it also drove its major drawbacks in a rehabilitation context because it requires repeated demands on an already impaired neuromuscular system [3, 7].

Two consequences follow. Sustained submaximal contraction accelerates the onset of neuromuscular fatigue, expressed as a decline in force-generating capacity together with a compression of the sEMG power spectrum toward lower frequencies [12]. The early stage of stroke rehabilitation faces a major obstacle because patients have weak voluntary muscle contractions and their bodies cannot activate enough motor units [2, 13]. Calibration contraction is no longer useful because fatigue results in non-stationarity; therefore, repeated calibrations are needed within the same session [3, 6, 11]. The system becomes unstable because the electrodes change position with the individual's limb, and contact resistance between the electrodes and the skin changes [14].

Pattern recognition methodology stems from an altogether different perspective. The system acquires feature vectors from small sliding windows and then classifies the motion patterns into one of a few predefined categories. The early stages of contraction exhibit a deterministic pattern which enables classification into categories using few channels of data [9, 10]. The user is therefore required only to generate an activation burst distinguishable from the background signal over a brief interval—135 ms in the implementation reported by Chen et al. [6]—with analysis windows of roughly 150–250 ms generally identified as the best compromise between class separability and perceived controller delay [15]. Once a class is detected, the device executes a pre-programmed trajectory without further volitional modulation [2, 3]. Three lines of evidence support the adoption of pattern recognition specifically for rehabilitation, as distinct from prosthetic applications:

- It preserves voluntary drive, consistent with the AAN paradigm. Assist-as-needed control requires that robotic assistance be scaled to the patient's residual voluntary effort, so that the device does not substitute for the neural drive that training is intended to elicit [7]. The rationale is empirical: actively generated movement produces greater cortical reorganization than passive movement matched for kinematics [8], and active practice is a precondition for the experience-dependent plasticity on which motor recovery depends. Research showed that EMG-driven robotic wrist training for patients with chronic stroke produced better results than continuous passive motion, which provided an equal amount of treatment [13]. The system requires activation bursts at the start of each movement because pattern recognition enforces this requirement directly rather than relying on automatic detection [3].

- The system establishes a motion path that follows biomechanical principles to achieve natural movement patterns. The clinical team sets predetermined movement routes for classified trajectories that maintain patient safety through correct anatomical positions during movement [2, 3]. This matters because hemiparetic reaching is characterized by stereotyped abnormal synergies: under continuous proportional control, the patient directly authors the trajectory and may therefore reinforce compensatory patterns, whereas a guided path constrains practice to the intended movement [7].
- It provides an explicit safety gate through reliable rest detection. Robust discrimination of a no-motion class is regarded as a prerequisite for clinically viable myoelectric control, since spurious actuation during intended rest is the failure mode most damaging to user trust [14]. Reported rest-detection accuracies approach 99% [6], yielding a discrete gate between intention and actuation. Continuous proportional control offers no equivalent gate, since any suprathreshold activity—including involuntary spasm or co-contraction—is translated into device motion [11].

Intent-based pattern recognition therefore offers a more natural and safer mode of human–device interaction for rehabilitation. However, much of this evidence derives from prosthetics research and healthy cohorts, and classification performance degrades in stroke populations: subject-specific classifiers applied to hemiparetic limbs have achieved approximately 71% accuracy in moderately impaired participants but below 40% in severely impaired participants [16]. The present study accordingly validates the integrated system in healthy participants as a necessary precursor to evaluation in the target clinical group.

## 3. Integrated System Description

### 3.1. Mechanical Subsystem

The exoskeleton offers five actuated revolute joints, which include Joint 0 (proximal/sternoclavicular approximation; range of motion ±5°), Joint 1 through Joint 3 (glenohumeral; range of motion 0–150°, ±90°, and −50° to +150° respectively), and Joint 4 (elbow flexion; range of motion 0–85°). The glenohumeral joints Joint 1, Joint 2, and Joint 3 have a common intersection point of the axes at the anatomical center of rotation, which allows the kinematic equivalence to a spherical joint of the glenohumeral joint. Importantly, all motors and links are located away from the point of intersection of the axes of the joints, thus shifting the mechanical mass laterally and inferiorly from the acromion point of view instead of being right on top of the shoulder joint. This is the main approach used to avoid the problem of head-and-torso collisions encountered by 3R mechanisms discussed in Section 2.1. The proximal joint J0 provides the sternoclavicular mobility that expands the functional workspace for cross-body and forward-reach motions and accommodates the scapulothoracic coupling observed during arm elevation. Fig. 4 shows the proposed shoulder mechanism. Three revolute joints

(J1, J2, J3), whose axes intersect at the glenohumeral COR, provide 3-DOF spherical motion. A fourth proximal joint (J0) approximates sternoclavicular/scapular mobility. The elbow joint (J4) completes the 5-joint chain. Motor and linkage offset from the COR reduce mechanical bulk over the acromion.

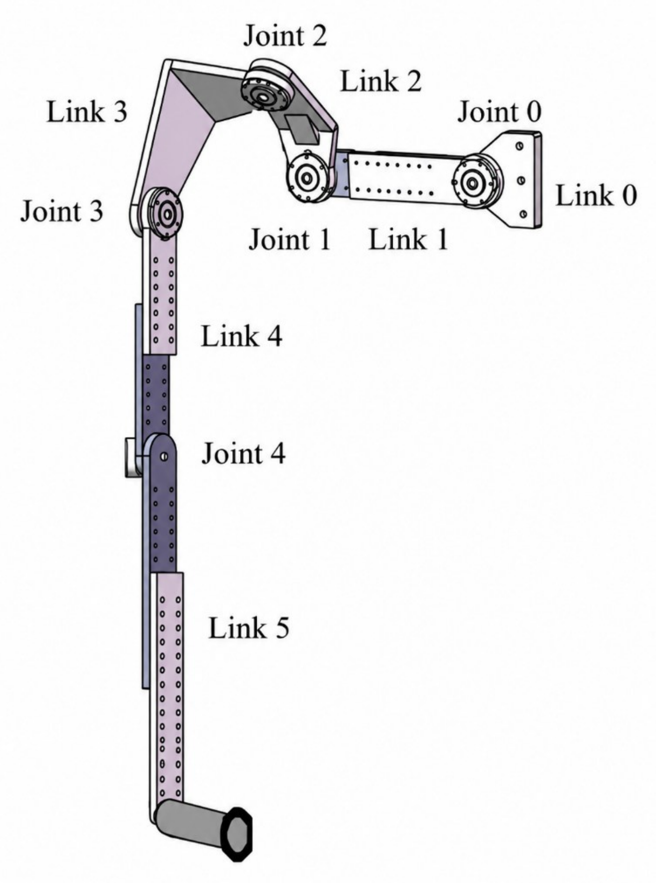


**Figure 4**. Proposed 4-DOF shoulder mechanism.

Each joint is driven by a Kollmorgen KH4248-B95020 closed-loop stepper motor (200 steps/rev, integrated encoder 1,000 counts/rev) coupled to a 1:100 planetary gearbox, yielding a peak joint torque of approximately 180 N·m and a maximum effective joint velocity of ≤60°/s. Closed-loop stepper motors were selected over conventional BLDC servo motors because they integrate the motor, encoder, and driver electronics into a compact unit and provide reliable position hold without active current at rest — eliminating the drift and low-frequency vibration that would degrade sEMG signals under continuous servo torque. A gear reduction of 1:100 was chosen to ensure the speed does not exceed safe limits for rehabilitation (shoulder: up to 60°/s; elbow: up to 30°/s).

Fig. 5 shows the physical prototype of the 4-DOF upper limb exoskeleton. Twelve Delsys Trigno Avanti wireless sEMG sensors (not shown) are placed at the shoulder, arm, and forearm positions. All structural components (links, brackets, motor mounts, and cuffs) were fabricated via fused deposition modeling (FDM) 3D printing using engineering-grade PETG polymer, with reinforced infill geometry in load-bearing zones. Telescoping aluminum segments in the upper arm and forearm provide anthropometric adjustability across the 5th–95th adult male percentile range. Complete device mass is 3.8 kg. The device is mounted on a height-adjustable aluminum stand for seated use; participants do not bear device weight on their own skeletal

https://doi.org/10.31436/iiumej.v27i3.4578

structure. Joint hard stops and software torque limits at 80% of stall torque implement dual independent safety layers.


**Figure 5**. Physical prototype of the 4-DOF upper limb exoskeleton.

### 3.2. sEMG Acquisition and Processing Subsystem

Twelve Delsys Trigno Avanti wireless sensors sample at 1,000 Hz per channel and stream data via TCP/IP over the Trigno SDK. Sensor placement follows SENIAM guidelines and covers the primary movers for all four ADL classes: middle and anterior deltoid, posterior deltoid, supraspinatus, pectoralis major, upper trapezius, infraspinatus, teres major, biceps brachii, triceps brachii, and flexor and extensor carpi radialis. Per-session baseline normalization (z-score using a 10-second rest recording prior to each block) compensates for inter-session skin impedance variation. Fig. 6 illustrates the data flow from the Trigno system to the LabVIEW processing pipeline. The Trigno SDK streams 12-channel sEMG data at 1,000 Hz on port 50043. A 500 ms circular buffer absorbs wireless packet jitter up to 18 ms peaks.

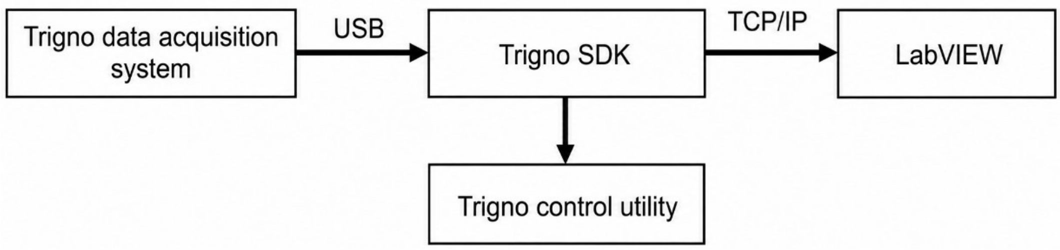


**Figure 6**. Data flow from the Delsys Trigno Avanti wireless sensor system to the LabVIEW acquisition loop via TCP/IP.

The LabVIEW processing pipeline runs in four parallel dataflow loops at tiered priorities, enabling concurrent acquisition, feature extraction, classification, and UI refresh without blocking. A 500 ms circular buffer absorbs Trigno wireless packet jitter of up to 18 ms peak while maintaining a continuous sample stream to the feature extraction loop. Feature extraction updates every 62.5 ms by computing six features per channel per 125 ms overlapping window: mean absolute value (MAV), root mean square (RMS), slope sign changes (SSC), Willison amplitude (WAMP), mean frequency (MNF), and median frequency (MDF), yielding a 72-dimensional feature vector. MAV and RMS characterize signal amplitude and correlate with muscle force; SSC and WAMP capture the frequency complexity of the signal burst; MNF and MDF characterize the spectral centroid and are sensitive to fatigue-induced spectral compression [12]. The time-domain subset follows the feature ensemble established by Hudgins et al. for multifunction myoelectric control [9], and the use of overlapping rather than disjoint windows with majority-vote post-processing follows the continuous-decision scheme of Englehart and Hudgins [10]. We deliberately chose the 125 ms window below the 150–250 ms range reported to minimize classification error [15], trading a small accuracy margin for reduced controller delay [15]. We selected the six features using offline optimization experiments, which showed better discriminative performance among the four ADL classes than models with fewer features. Predictions are stabilized by taking a majority vote of three consecutive predictions (within 187.5 ms). The predicted intent is sent to the Arduino through the USB serial connection (115,200 baud rate). Fig. 7 illustrates the entire process flow of online pattern recognition of sEMG signals. The twelve-channel sEMG signals are captured and processed with a window size of 125 ms and an interval of 62.5 ms to generate a 72-dimensional vector at each 62.5 ms interval.

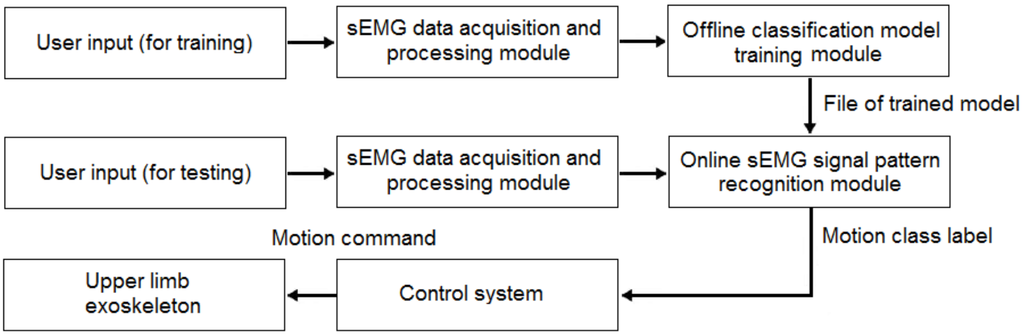


**Figure 7**. Online sEMG pattern recognition workflow implemented in LabVIEW.

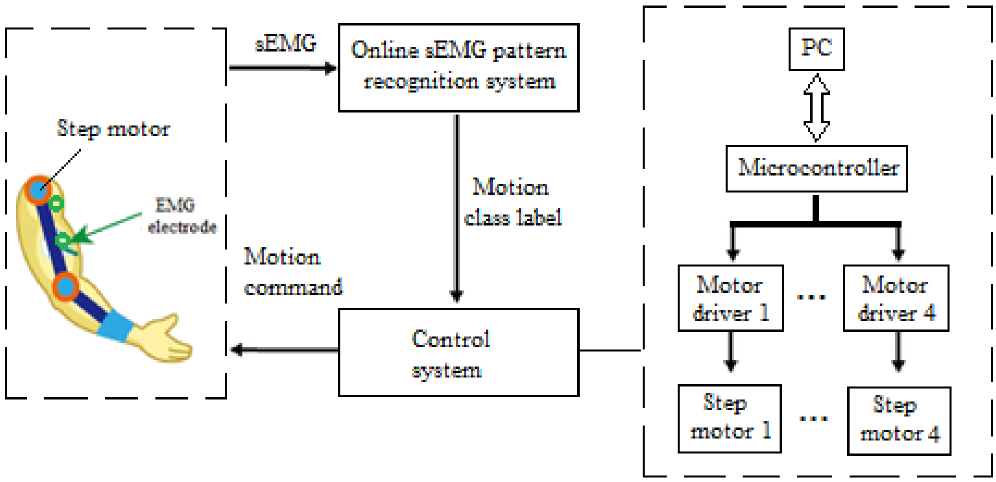


**Figure 8**. Integrated system architecture.

Figure 8 illustrates the system architecture. Three separate loops in LabVIEW run in parallel (acquisition loop, feature extraction/classification loop, and command generation loop) and exchange data through internal queues. Communication is enabled through external interfaces such as TCP/IP (Delsys Trigno SDK) and USB serial communication (Arduino Mega 2560).

### 3.3. Kinematic Modeling and Simulation

The 5-joint kinematic chain was modeled mathematically using the Denavit–Hartenberg (DH) convention, where coordinate frames were defined for each joint. Since J1, J2, and J3 have their centers of rotation (COR) coinciding with that of the glenohumeral joint, their coordinate frames have their origin at the same point and hence have link offsets of zero in the DH parameter table. The mathematical modeling of the 5-joint chain was done using MATLAB's Robotics Toolbox, where the Link and SerialLink objects were used with parameters derived from the SolidWorks CAD model. Joint range of motion limits were derived based on population-based anthropometric data, which are: J0 (+/-5°), J1 (0°-150°), J2 (+/-90°), J3 (-50°-150°), J4 (0°-85°). Figure 9 shows the kinematic model and its workspace, respectively.

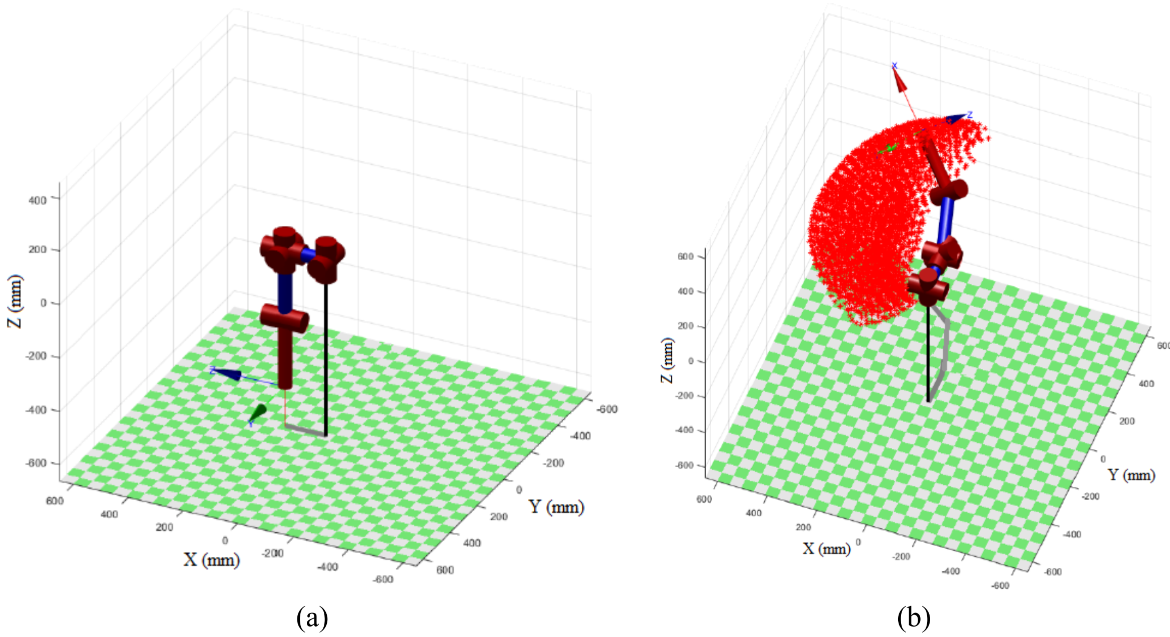


**Figure 9**. Kinematic modeling and workspace simulation of the five-joint upper-limb exoskeleton: (a) DH-based kinematic model implemented in MATLAB Robotics Toolbox and (b) simulated end-effector workspace.

### 3.4. Low-Level Actuation Subsystem

Four Summtor MB 450A stepper motor drivers receive step and direction pulses from the Arduino Mega 2560. The Arduino converts each incoming ASCII intention command from LabVIEW into a preset joint trajectory programmed into the firmware, as a sequence of angular waypoints at 24°/s. Trajectories were designed collaboratively with a physiotherapist to match normative upper limb kinematics for each ADL: SAB guides J1 from 0° to 90° in the frontal plane with accompanying scapular elevation compensation through J0; PUC executes combined J1 shoulder flexion to 45° and J4 elbow flexion to 70°; PFC executes J1 shoulder flexion to 60° while maintaining elbow near-extension; RA issues a STOP command and holds the current position with motor holding torque. Trapezoidal velocity profiles (30°/s$^2$ ramp-up and ramp-down) prevent jerk at movement initiation and termination.

## 4. Experimental Methods

The validation followed a five-step workflow (see Fig. 10) in which each subsystem was assessed both on its own and in combination. The mechanical subsystem was first characterized in isolation through kinematic modeling and workspace simulation (Section 3.3); the sEMG intent-recognition pipeline was first evaluated as a standalone classifier on previously recorded offline data from the same volunteers; the two were then brought together in the integrated, physically coupled closed-loop setup described below; and finally the standalone and integrated conditions were cross-validated using the identical set of participants. Because the same individuals were tested offline, in free space, and under physical coupling, each participant serves as their own control, so any change in classification accuracy or signal quality can be attributed to the physical coupling itself rather than to between-subject variability. This within-subject cross-validation provides tighter control than validating the mechanism and the classifier on separate cohorts, and it underpins the signal-quality comparison reported in Section 5.2.

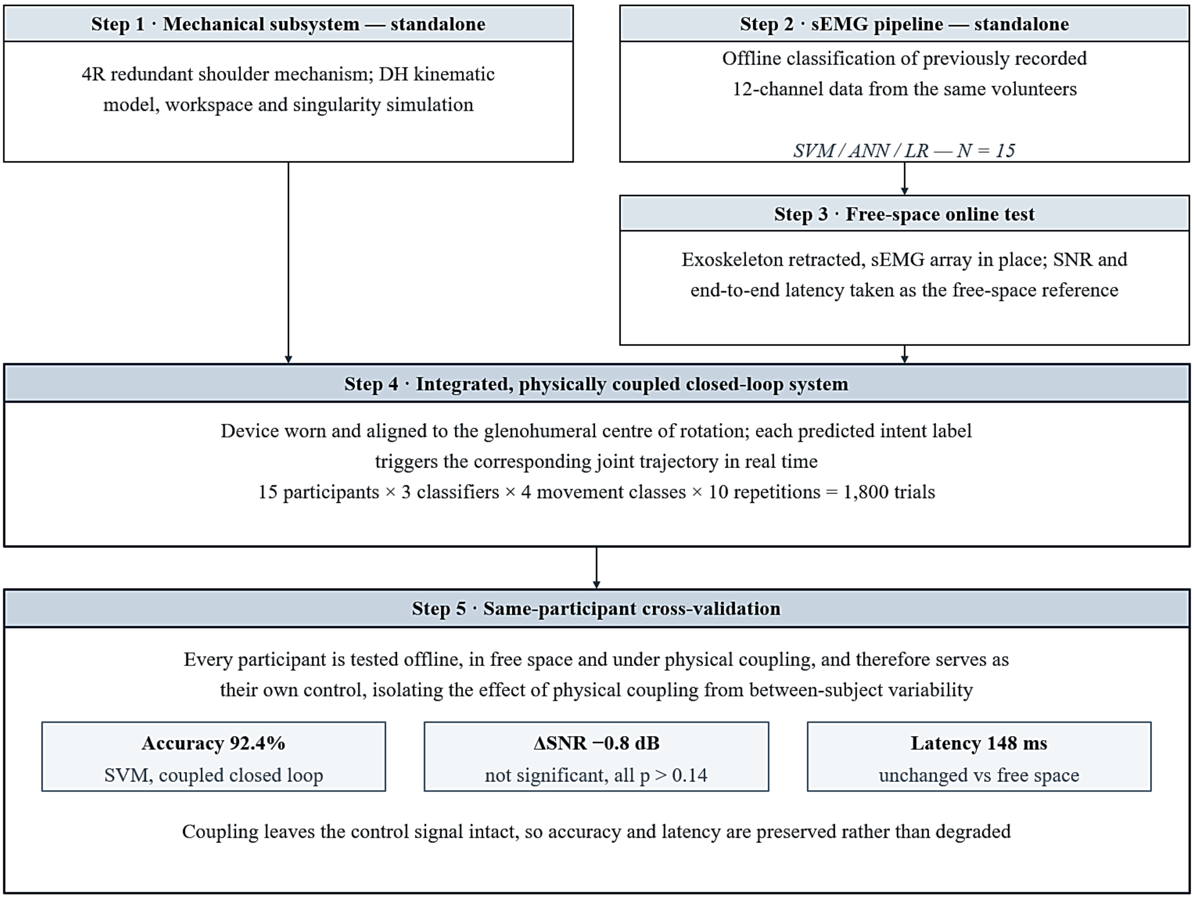


**Figure 10**. Staged validation workflow.

## 4.1. Participants

A total of fifteen healthy volunteers were included (10 males, 5 females; aged 23 ± 3.7 years; stature 1.71 ± 0.14 m; body weight 67.2 ± 4.8 kg). All had taken part in the earlier offline dataset study, so that the offline, free-space, and physically coupled conditions were assessed within the same individuals. Subjects with neuromuscular diseases, arm injuries within the past 12 months, and/or those with conditions influencing the voluntary control of movements and sEMG signals were excluded. The Institutional Research Ethics Committee reviewed and approved all experimental procedures involving human participants (approval no. MREC/AS/25/26/006), and the study was conducted in accordance with the Declaration of Helsinki. Written informed consent was obtained from every participant prior to enrolment.

https://doi.org/10.31436/iiumej.v27i3.4578

This was a non-clinical pilot study conducted with healthy volunteers under the appropriate institutional clearance.

### 4.2. Movement Set and Clinical Rationale

Four movement classes were evaluated and chosen for their clinical importance in early post-stroke upper limb rehabilitation. Pilot testing also confirmed they were feasible within the device's range of motion. Shoulder abduction (SAB, 0–90° frontal plane) is an isolated proximal movement closely tied to regaining anti-gravity control after a stroke. "Pick up a cup" (PUC) – shoulder flexion and elbow flexion movements for reaching, grasping, and lifting a 50 g foam cup that is placed 30 cm anteriorly – is a basic task of reach and grasp activity of daily living used in a number of standardized tests (ARAT, WMFT). Pushing a cup forward (PFC) includes pushing the cup 30 cm anteriorly on the table using a flat palm of the hand. It uses similar proximal musculature as PUC but different distal musculature. Resting arm (RA) is a relaxed arm hanging down at the side. This is a crucial safety point; good recall of RA will protect against accidental device activation.

### 4.3. Experimental Protocol

Each participant underwent one session of integration, which lasted about 125 minutes, in four steps:

- Step 1 – Device fitting and familiarization (20 min). The alignment of the glenohumeral COR was checked by aligning the point of crossing of the J1- J3 axes with respect to a calibration marker placed over the acromion process of the subject. The link length of the device was adjusted such that it was equal to the length of the subject's upper arm and forearm segments, respectively. Each subject performed each action three times without the sEMG pipeline to become accustomed to the movement mechanism.
- Stage 2 — Free-space reference block (15 min). Before coupling the exoskeleton to the limb, participants performed 10 repetitions of each of the four movement classes with the twelve-channel sEMG array in place, the device retracted, and the arm moving unconstrained in free space. Acquisition, feature extraction, and classification ran with settings identical to the coupled condition, but no motor commands were issued. This block provided the free-space reference for the per-channel SNR comparison reported in Section 5.2 and the end-to-end latency comparison reported in Section 5.3.
- Stage 3 — Evaluation of classifiers (80 min). Evaluation of classifiers was done in three blocks (SVM, ANN, and LR, respectively) in counterbalanced order across subjects, with a rest of 10 minutes for every two successive blocks, totaling 80 min in Stage 3, i.e., (3 × 20 min) + (2 × 10 min) = 80 min. Within each block, participants performed 10 repetitions of each of the four movement classes (40 trials per block, 120 trials per participant, 1,800 trials in total across the 15 participants) in a randomized block design cued by a visual display. This was a fully closed-loop system, meaning that every prediction of an intent label was associated with the predefined motor trajectory that the device followed. The repetitions were spaced with a 5-second break, and there were 10-minute breaks after each classifier block.
- Stage 4 — Usability and comfort questionnaires (10 min).

### 4.4. Outcome Measures

Intent Recognition Accuracy: Accuracy, Precision, Recall, and F1 Scores for each classifier were calculated across all subjects and runs. An intent was accurately recognized if the majority vote label in the cue movement window was equal to the instructed class label. End-to-end latency was defined as the interval from EMG burst onset — detected using a double-threshold algorithm (RMS envelope >3 SD above baseline, sustained ≥20 ms) — to the Arduino serial command timestamp, measured using LabVIEW microsecond-resolution Tick Count primitives. Signal quality: Per-channel SNR was computed as the ratio of mean RMS amplitude during active movement windows to mean RMS during RA windows (dB scale), compared between physically coupled and free-space conditions (the free-space reference being the Stage 2 block described in Section 4.3) using 12 paired t-tests with Bonferroni correction (adjusted $\alpha = 0.004$). Usability: System Usability Scale (SUS, 10 items, 0–100; scores of approximately 68 and above correspond to a "Good" rating on the Bangor et al. adjective-rating scale [17]). Discomfort: Numeric Rating Scale (NRS, 0–10) at three attachment sites. Compensatory movement: A physiotherapist observer recorded trunk lean or shoulder shrug (blinded to classifier block order).

### 4.5. Statistical Analysis

Classifier effects on accuracy and latency were evaluated using one-way repeated-measures ANOVA with Greenhouse–Geisser correction for sphericity violations and Bonferroni post-hoc pairwise comparisons. Free-space-to-coupled accuracy degradation was tested with paired t-tests. Effect sizes were reported as partial eta-squared ($\eta^2 p$) for ANOVA and Cohen's d for pairwise tests. The significance threshold was $\alpha = 0.05$. All analyses were performed in MATLAB R2023b.

## 5. RESULTS

### 5.1. Intent-Recognition Accuracy

Table 1 situates the present system within a representative set of recently reported integrated sEMG-controlled upper limb exoskeletons. The comparison is restricted to recent systems that pair a physically worn mechanism with an sEMG-driven control model, because classifier accuracies reported on disembodied benchmark recordings are not directly comparable to values obtained during active, physically coupled device use. The set is nevertheless heterogeneous: not every system actuates the shoulder, and not everyone classifies movement intent online, as noted below. Across this set, the present system is the only one to report an end-to-end online latency measured under full physical coupling (148 ms), and the only one to quantify the effect of that coupling on sEMG signal quality directly. Its online accuracy of 92.4% is obtained with the mechanism worn and moving.

A few caveats apply in making this comparison and are highlighted here to avoid overstating the outcome. First, the present study classifies four movement classes, fewer than the five [20] and six [18] used elsewhere. Because class separability generally decreases as classes are added, part of the accuracy difference reflects the smaller decision space rather than the system itself. Similarly, the nominal number of DOF in the shoulder joints in this study differs from those of the other approaches, as this study uses a redundant 4-DOF configuration that utilizes the redundancy to perform singularity and collision avoidance for the shoulder (see Section 2.2), while the number of DOFs in the other approaches describes the kinematic configuration of the system. Zhao et al. [20] report higher accuracy than the present system, but on offline recordings and over activity and load states rather than discrete ADL movement classes. Regarding response time, the present study is the only system in Table 1 to report end-to-end latency (148 ms, below the 200 ms threshold); the remaining systems did not report latency (listed as N/R in Table 1), so a direct latency comparison is not possible. Taken together, the present system is the only entry in Table 1 that combines a redundant 4-DOF shoulder mechanism, full physical coupling during evaluation, a reported sub-150 ms end-to-end latency, and the highest online accuracy among the systems evaluated under physical coupling.

**Table 1**. Representative integrated sEMG-controlled ULE systems compared with the present study

| System | DOFs (shoulder) | Classifier | Classes | Reported acc. % | Latency (ms) | Physical coupling |
|---|---|---|---|---|---|---|
| Guo et al. [18] | N/R | SVM | 6 | 79 | N/R | Yes — robotic arm |
| Trigili et al. [19] | 4 | GMM | N/R | N/R | N/R | Yes — full |
| Zhao et al. [20] | N/R | CNN-BiLSTM-attention | 5 | 97.3 / 88.2 | N/R | Yes — full (offline) |
| **Present study** | **4** | **SVM/ANN/LR** | **4** | **92.4** | **148** | **Yes — full, physical** |

*SVM: support vector machine; ANN: artificial neural network; CNN: convolutional neural network; LSTM: long short-term memory network. Accuracies are as reported by the original authors. Zhao et al. [20] evaluated offline; their two values are the within-subject test-set and leave-one-subject-out cross-validation accuracies, respectively.*

Table 2 reports overall and per-class classifier accuracy under physically coupled closed-loop conditions. One-way repeated measures ANOVA indicated a significant effect of classifier on accuracy ($F(2,28) = 19.3$, $p < 0.001$, $\eta^2 p = 0.58$). Post hoc tests: SVM > ANN (mean difference 2.7%, $p = 0.003$, $d = 0.54$); SVM > LR (7.3%, $p < 0.001$, $d = 1.14$); ANN > LR (4.6%, $p < 0.001$, $d = 0.71$). SVM accuracy exceeded 80% for all 15 participants.

**Table 2**. Closed-loop intent-recognition performance (mean ± SD, N = 15). Best values per metric in bold

| Metric | SVM (linear) | ANN (MLP) | LR |
|---|---|---|---|
| **Overall accuracy (%)** | 92.4 ± 4.1 | 89.7 ± 5.8 | 85.1 ± 6.9 |
| **SAB recall (%)** | 96.0 ± 3.8 | 95.0 ± 4.1 | 86.0 ± 6.2 |
| **PUC recall (%)** | 86.0 ± 6.7 | 78.0 ± 8.4 | 70.0 ± 9.3 |
| **PFC recall (%)** | 82.0 ± 7.4 | 76.0 ± 8.1 | 72.0 ± 8.8 |
| **RA recall (%)** | 98.0 ± 2.1 | 97.0 ± 2.6 | 96.0 ± 3.0 |
| **Mean precision (%)** | 88.1 ± 5.2 | 85.6 ± 6.0 | 80.6 ± 7.5 |
| **Mean F1 score (%)** | 90.3 ± 4.6 | 87.4 ± 5.9 | 82.8 ± 7.1 |
| **End-to-end latency (ms)** | 148 ± 19 | 158 ± 23 | 155 ± 22 |
| **SUS score (0–100)** | 71.3 ± 8.4 | 68.9 ± 9.1 | 66.2 ± 10.7 |

*SVM: support vector machine (linear kernel, one-vs-one); ANN: multilayer perceptron (20 neurons, ReLU, softmax); LR: logistic regression (one-vs-rest).*

Classifier performance in terms of precision and recall is shown in Fig. 11. The main issue across all classifiers is confusion between PUC and PFC tasks (for SVM, 9% PUC classified as PFC and 10% PFC classified as PUC), which relates to the common forward-reach part of the task in which both muscles are engaged. All three classifiers perform best for the RA and SAB classes.

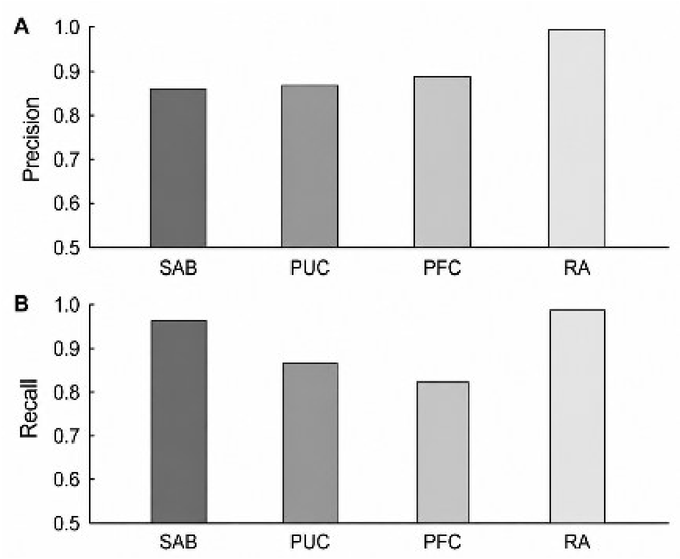


(a)

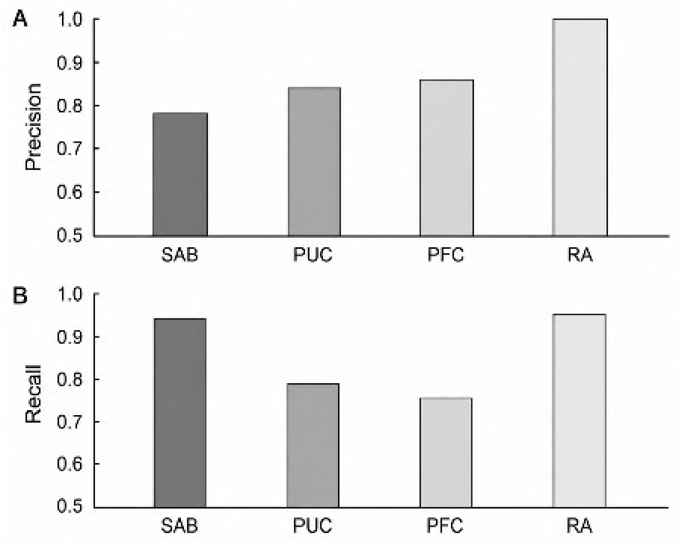


(b)

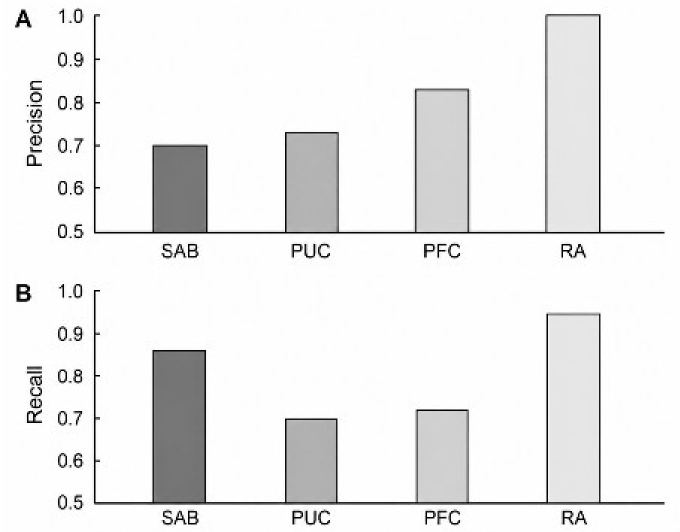


(c)

**Figure 11**. Class-wise precision and recall of the three classifiers: (a) support vector machine (SVM), (b) artificial neural network (ANN), and (c) logistic regression (LR).

https://doi.org/10.31436/iiumej.v27i3.4578

### 5.2. Effect of Physical Coupling on sEMG Signal Quality

Table 3 presents per-channel SNR under physically coupled (device worn) and free-space (device absent) conditions. The mean SNR decrease of −0.8 dB under physical coupling was not statistically significant after Bonferroni correction (corrected threshold $p < 0.004$; all $p > 0.14$). This confirms that the 4-DOF mechanism's anatomical alignment prevents the vibration-induced and shear-induced electrode displacement that would substantially degrade sEMG quality in a mechanically misaligned device.

**Table 3**. Per-channel SNR (dB, mean ± SD, N = 15) under free-space and physically coupled conditions

| Ch. | Muscle | Free-space SNR (dB) | Coupled SNR (dB) | ΔSNR (dB) | p-value |
|---|---|---|---|---|---|
| 1 | Middle deltoid | 18.4 ± 3.2 | 17.6 ± 3.8 | −0.8 | 0.19 |
| 2 | Anterior deltoid | 17.1 ± 2.9 | 16.2 ± 3.4 | −0.9 | 0.14 |
| 3 | Posterior deltoid | 16.8 ± 3.1 | 15.9 ± 3.6 | −0.9 | 0.17 |
| 4 | Supraspinatus | 14.2 ± 3.7 | 13.4 ± 4.1 | −0.8 | 0.22 |
| 5 | Pectoralis major | 19.3 ± 2.8 | 18.7 ± 3.1 | −0.6 | 0.31 |
| 6 | Trapezius (upper) | 15.7 ± 3.4 | 14.9 ± 3.9 | −0.8 | 0.21 |
| 7 | Infraspinatus | 13.9 ± 4.0 | 13.1 ± 4.4 | −0.8 | 0.24 |
| 8 | Teres major | 14.6 ± 3.5 | 13.8 ± 3.9 | −0.8 | 0.20 |
| 9 | Biceps brachii | 20.1 ± 2.6 | 19.4 ± 2.9 | −0.7 | 0.26 |
| 10 | Triceps brachii | 17.8 ± 3.0 | 17.0 ± 3.4 | −0.8 | 0.18 |
| 11 | Wrist flexor (FCR) | 16.5 ± 3.2 | 15.8 ± 3.6 | −0.7 | 0.27 |
| 12 | Wrist extensor (ECR) | 15.9 ± 3.3 | 15.2 ± 3.7 | −0.7 | 0.25 |
| **Mean** | **All channels** | **16.7 ± 3.2** | **15.9 ± 3.6** | **−0.8** | **0.21** |

*ΔSNR = coupled minus free-space. No comparison reached significance after Bonferroni correction (corrected p < 0.004; all p > 0.14).*

### 5.3. End-to-End Latency

SVM latency under physical coupling was 148 ± 19 ms — identical within measurement uncertainty to free-space conditions. ANN (158 ± 23 ms) and LR (155 ± 22 ms) were similarly unchanged. A paired t-test confirmed no significant difference between coupled and free-space latency for SVM ($t(14) = 0.41$, $p = 0.69$). All three classifiers remained below the 200 ms therapeutic latency threshold in every session and every participant [15]. The dominant latency contributor was the windowing stage (~60 ms, accounting for >40% of total latency), confirming that reducing window length — rather than faster classifiers — is the primary lever for further latency reduction.

### 5.4. Usability, Comfort, and Compensatory Movement

SUS mean scores when using the SVM control were 71.3 ± 8.4, classified as "Good" on the adjective rating scale [17]. The mean scores for ANN and LR were 68.9 ± 9.1 and 66.2 ± 10.7, respectively. The effect of the classifier on the SUS score was statistically significant ($F(2,28) = 4.87$, $p = 0.015$, $\eta^2p = 0.26$). The SVM classifier achieved a significantly higher SUS score than LR ($p = 0.008$, $d = 0.55$), as participants indicated that it provided faster and more reliable classification of their intent, minimizing uncertainty about the device's recognition success. The mean discomfort NRS score was 1.8 ± 0.7. No participant got an NRS score of 4. Three participants reported a mild, temporary tingling sensation within the first five minutes of use. The compensation rate during the SAB task was 4.1% (in some cases above 80° of abduction) and 2.8% during the PUC task, resulting in a mean rate of 3.5%.

## 6. DISCUSSION

### 6.1. Integration Findings: Mechanical–Signal Interaction

The primary integration result is that physical coupling had little effect on sEMG signal quality: the mean ΔSNR was −0.8 dB for all twelve channels (Table 3). Hence, mechanical coupling introduced no noticeable electrical noise [4]. Importantly, the preservation of the quality of the signal is the basis by which the results of the mechanical and classification experiments can be linked to each other: because the coupling has not led to SNR degradation, the classifier has processed the signals in much the same way as it does in free space, which is the reason why the accuracy of the closed loop remained at the level of 92.4%, and the latency of the loop was 148 ms. Thus, the results demonstrate the effectiveness of the anatomically matched shoulder design in reducing the electrode displacement that conventional upper-limb exoskeletons experience [4, 5, 14]. Conventional designs confine shoulder movement to a fixed mechanical pivot and do not allow the glenohumeral joint COR to shift [5]. This kinematic mismatch generates interaction forces that lead to shear force, increased skin pressure, electrode displacement, and ultimately device rejection or joint injury [4, 5].

The lack of signal degradation shows that matching the mechanism with the COR eliminates the displacement mechanism and preserves signal quality [4]. This supports perceptual transparency: mechanical coupling has not destroyed the physiological signal on which intent recognition relies [4]. According to the results published by Pan et al. [4], self-aligning designs with passive DOFs allow keeping the glenohumeral rotation deviations within approximately 20 mm and having the same muscle activation patterns as in the case of no load, while fixed-axis designs cause the trajectory deviation up to 50 mm and greatly increase peak activation of the deltoid and upper trapezius muscles [8].

The practical implication of integrating the two subsystems in the experiment is that each subsystem's results would be meaningless on its own. Classifier accuracy measured in free space provides no guarantee that it persists when electrodes are loaded and the device vibrates, while the kinematic compatibility test results provide no guarantee that the remaining misalignment is small enough to allow use of the control signal.

### 6.2. System Responsiveness and Clinical Deployment

The mean latency of 148 ms matters for safe and intuitive physical human–robot interaction, since assistive responses must fall within biologically natural timing [3, 15]. This latency remains significantly below the accepted 200 ms threshold for implementing natural assistive responses in real-time control [3]. The stability of latency in free-space and coupled conditions (Section 5.3) shows that the device's mechanical structure does not introduce vibration noise or computational delay in the real-time loop [4, 6].

This responsiveness follows from using computationally inexpensive time-domain features with a classical classifier: linear SVMs have been reported to reach online accuracies of approximately 90% for upper limb movement classification, comparable to more complex models [3, 6, 14]. Deep learning architectures achieve high classification accuracy but impose substantial computational demands and end-to-end latencies of 200–500 ms [3]. Avoiding architectures that require GPU acceleration therefore allows stable operation on standard laboratory hardware, which matters for eventual clinical deployment [3, 6].

### 6.3. Implications for Intent-Driven Rehabilitation

The findings show that a 4-DOF mechanism can be combined with real-time intent recognition for functional ADL tasks [3, 6]. Preserving sEMG integrity under mechanical loading allows the user to remain an active participant in the movement, which is a precondition for regaining motor control [7, 8]. These findings align with contemporary neurorehabilitation theory, which states that voluntary patient involvement helps facilitate neuroplasticity [13]. Because this validation was limited to a single seated laboratory session, robustness across different environments and repeated daily sessions has not yet been established; domain-adaptation methods are therefore a promising direction for future work to address inter-session and inter-environment variability [14].

### 6.4. Biomechanical Interpretation of the PUC–PFC Confusion

The 9–10% mutual misclassification between picking up a cup (PUC) and pushing a cup forward (PFC) under SVM is consistent with the biomechanical literature on upper limb task initiation [6]. PUC and PFC both involve an initial reaching phase in an identical arc of shoulder flexion, powered mainly by the anterior deltoid and pectoralis major muscles [2, 3]. During this initial phase, the two tasks are kinematically indistinguishable, producing substantial overlap in activation patterns that no classifier can resolve from proximal channels alone [3, 6, 14].

The discriminating features are distal: flexor carpi radialis activation in preparation for grasping in PUC, and extensor carpi radialis activation for flat-palm pushing in PFC [6]. Because these muscles activate late in both movements, they fall outside the 125–135 ms analysis window anchored at movement onset [6, 9]. A short window is necessary to keep latency below the 200 ms therapeutic thresholds, but it cannot capture the late activation needed to separate functionally similar reach-to-grasp and reach-to-push intentions [3, 6, 15].

Solving this issue will require more sensing modalities that provide contextual information [3]. IMUs or force sensors can monitor joint coordination and interaction forces before distal muscle activation [3, 6]. Moreover, a hierarchy-based classification process may place more importance on distal cues as motion progresses, leading to better intention estimation [3]. This is one way perceptual transparency can be achieved in such a system [4].

### 6.5. Pattern Recognition vs. Proportional Control: Evidence Analysis

Experimental findings provide empirical evidence to compare PR and proportional control through five dimensions. The first dimension is effort demands. Participants experienced no difficulty (NRS 1.8) during 20 minutes of continuous task performance, with compensatory movements occurring in just 3.5% of all trials, indicating low effort demands. Proportional control depends on calibrated muscle contraction for every 2- to 4-second trial period, requiring much more physical effort from the participant. The low effort demand and near absence of compensatory movement align with the clinical requirement for low-effort practice in early post-stroke rehabilitation [2, 3]. In contrast, proportional control relies on sustained, calibrated muscle contractions to change the torque level, whereas PR requires only a burst of volitionally initiated muscular contractions [6, 11]. This difference matters because physical fatigue is a major obstacle during stroke rehabilitation, often changing the characteristics of the bioelectrical signal and requiring continuous recalibration in proportional control systems [3], [12]. By shortening the required contraction, pattern recognition mitigates the fatigue effects that otherwise degrade task performance and contribute to device rejection [3].

The second dimension is trajectory quality. Each SAB repetition follows an identical physiotherapist-designed frontal plane arc at 24°/s irrespective of the amplitude modulation. Each repetition therefore follows a physiotherapist-designed path whose biomechanical correctness does not depend on the participant's instantaneous EMG amplitude. A stable, guided path provides the repeatability required for both training and quantitative assessment. According to the literature, such guidance protects against reinforcing spastic synergies or motor maladaptation that could occur when a patient with limited coordination guides the proportional system [2, 3].

Third, calibration stability. Session-based baseline normalization maintained accuracy for all fifteen participants across 20-minute blocks without recalibration. In contrast, the proportional control requires MVC calibration for each channel with recalibration when amplitude drift occurs. The PR framework's stability over 20 minutes without recalibration solves one of the biggest technical problems in wearable robotics [3]. Traditional proportional myoelectric control is extremely sensitive to non-stationarity, drift, and bioelectrical signal changes caused by fatigue, requiring repeated Maximum Voluntary Contraction (MVC) tests that take valuable clinical time [3, 6, 11]. Using session-based normalization and computationally efficient time-domain features, the PR systems maintain higher long-term accuracy, making them deployable in resource-limited clinical environments [6].

Fourth, safety. Recall of 98% for the resting arm (RA) class corresponds to unintended actuation in only 2% of rest periods, and constitutes the safety gate on which clinically viable myoelectric control depends [6]. According to research, reliable intention recognition requires robust rest detection, with benchmarks up to 99%, to avoid the unintended actuation inherent to continuous proportional controllers [6, 14]. This way, the exoskeleton stays inactive during involuntary muscle spasms or other unintended movements, improving interaction safety during rehabilitation.

Fifth, active engagement. Requiring a volitional burst before each movement satisfies the assist-as-needed principle, under which robotic assistance is provided in proportion to the user's own effort [3]. Contemporary neurorehabilitation theory states that active volitional engagement is the prerequisite for cortical reorganization and durable functional recovery [2, 8]. By positioning the patient as an active agent rather than a passive recipient of movement, pattern-recognition control engages the neuroplastic processes on which motor recovery depends [2, 3, 13].

### 6.6. Limitations and Future Work

Four key restrictions need to be recognized. First, the study subjects were healthy young adults. Patients who have suffered stroke, with spasticity, co-contraction, and abnormal muscle synergies show a very different set of sEMG characteristics, especially in more complex movements such as PUC and PFC, where distal selectivity is the bottleneck; subject-specific classifiers applied to hemiparetic limbs have reported approximately 71% accuracy in moderately impaired participants and below 40% in severely impaired participants [16]. Extending to post-stroke subjects is the main next step and will require an adaptive or transfer-learning classifier approach due to large inter-subject and inter-session variability in the population. Second, each classifier block lasted 20 minutes, and all blocks were completed on a single day; inter-day variability in electrode placement and classifier performance in multi-session protocols has not been characterized. Third, the stand-mounted system does not have subjects bear the weight of the device through their own skeleton; back-mounted or orthotic mounting will change the weight-bearing properties of the shoulder mechanism and the electrode array. Fourth, the wrist was not actuated, so it cannot produce the coordinated wrist and hand motion required for many ADLs.

## 7. CONCLUSION

This paper presented a fully integrated, sEMG-controlled 4-DOF upper limb exoskeleton intended for post-stroke rehabilitation, and validated it experimentally in healthy participants as a proof of concept. The system combines a novel shoulder mechanism — three glenohumeral revolute joints with co-located axes at the anatomical COR and a proximal sternoclavicular-replicating joint — with a LabVIEW-based real-time sEMG pipeline classifying four functional ADL classes using a linear SVM on 72-dimensional feature vectors extracted every 62.5 ms.

In a closed-loop experiment with 15 healthy participants physically wearing and using the device, the system achieved 92.4% overall intent-recognition accuracy, with 96% recall for SAB and 98% recall for RA—the highest online accuracy among comparable systems in Table 1 evaluated under physical coupling. End-to-end latency was 148 ± 19 ms, below the 200 ms therapeutic threshold. Physical coupling produced no statistically significant sEMG degradation (mean ΔSNR −0.8 dB, all $p > 0.14$ after Bonferroni correction), demonstrating that anatomical alignment directly preserves signal quality. Participants rated usability as "Good" (SUS 71.3) and reported only mild discomfort (NRS 1.8). Compensatory movement was observed in 3.5% of trials, substantially below rates reported for misaligned designs.

In summary, anatomically aligned mechanical design and lightweight sEMG pattern recognition are complementary: the same joint alignment that reduces parasitic interaction forces also limits electrode displacement, so the classifier receives cleaner signals than a mechanically coupled but misaligned device would deliver. The next phase will involve chronic stroke patients, expanding the range of movements from four to seven classes or more, and incorporating instrumented cuffs.

## ACKNOWLEDGEMENT

The authors thank the 15 participants for their time and commitment at Xi'an Peihua University for professional guidance in trajectory design and compensatory movement assessment.

## REFERENCES

[1] Feigin VL, Brainin M, Norrving B, Martins S, Sacco RL, Hacke W, Fisher M, Pandian J, Lindsay P (2022) World Stroke Organization (WSO): Global stroke fact sheet 2022. Int. J. Stroke, 17(1):18-29. https://doi.org/10.1177/17474930211065917

[2] Hasan SK, Bhujel SB, Niemiec GS (2024) Emerging trends in human upper extremity rehabilitation robot. Cognit. Robot., 4:174-190. https://doi.org/10.1016/j.cogr.2024.09.001

[3] Karasheva M, Saudanbekova A, Utepbergen A, Akkulova S, Niyetkaliyev A, Ozhikenov K, Ozhiken A, Alimbayev C, Shylmyrza U, Aimukhanbetov Y (2025) Sensor-driven control strategies for post-stroke shoulder rehabilitation exoskeletons: A systematic review. MethodsX, 15:103648. https://doi.org/10.1016/j.mex.2025.103648

[4] Pan J, Astarita D, Baldoni A, Dell'Agnello F, Crea S, Vitiello N, Trigili E (2023) A self-aligning upper-limb exoskeleton preserving natural shoulder movements: Kinematic compatibility analysis. IEEE Trans. Neural Syst. Rehabil. Eng., 31:4954-4964. https://doi.org/10.1109/TNSRE.2023.3341219

[5] Pramod AS, Mohan S, Thondiyath A (2025) A modified human shoulder model considering the migration of the humeral head from the scapular glenoid fossa for the design of shoulder exoskeletons. Proc. Inst. Mech. Eng. C J. Mech. Eng. Sci., 239(5):1441-1456. https://doi.org/10.1177/09544062241295631

[6] Chen B, Zhou Y, Chen C, Sayeed Z, Hu J, Qi J, Frush T, Goitz H, Hovorka J, Cheng M, Palacio C (2023) Volitional control of upper-limb exoskeleton empowered by EMG sensors and machine learning computing. Array, 17:100277. https://doi.org/10.1016/j.array.2023.100277

[7] Marchal-Crespo L, Reinkensmeyer DJ (2009) Review of control strategies for robotic movement training after neurologic injury. J. NeuroEngineering Rehabil., 6:20. https://doi.org/10.1186/1743-0003-6-2

[8] Lotze M, Braun C, Birbaumer N, Anders S, Cohen LG (2003) Motor learning elicited by voluntary drive. Brain, 126(4):866-872. https://doi.org/10.1093/brain/awg079

[9] Hudgins B, Parker P, Scott RN (1993) A new strategy for multifunction myoelectric control. IEEE Trans. Biomed. Eng., 40(1):82-94. https://doi.org/10.1109/10.20477

[10] Englehart K, Hudgins B (2003) A robust, real-time control scheme for multifunction myoelectric control. IEEE Trans. Biomed. Eng., 50(7):848-854. https://doi.org/10.1109/TBME.2003.813539

[11] Fougner A, Stavdahl Ø, Kyberd PJ, Losier YG, Parker PA (2012) Control of upper limb prostheses: Terminology and proportional myoelectric control—A review. IEEE Trans. Neural Syst. Rehabil. Eng., 20(5):663-677. https://doi.org/10.1109/TNSRE.2012.2196711

[12] Enoka RM, Duchateau J (2008) Muscle fatigue: What, why and how it influences muscle function. J. Physiol., 586(1):11-23. https://doi.org/10.1113/jphysiol.2007.139477

[13] Hu XL, Tong KY, Song R, Zheng XJ, Leung WWF (2009) A comparison between electromyography-driven robot and passive motion device on wrist rehabilitation for chronic stroke. Neurorehabil. Neural Repair, 23(8):837-846. https://doi.org/10.1177/1545968309338191

[14] Scheme E, Englehart K (2011) Electromyogram pattern recognition for control of powered upper-limb prostheses: State of the art and challenges for clinical use. J. Rehabil. Res. Dev., 48(6):643-659. https://doi.org/10.1682/JRRD.2010.09.0177

[15] Smith LH, Hargrove LJ, Lock BA, Kuiken TA (2011) Determining the optimal window length for pattern recognition-based myoelectric control: Balancing the competing effects of classification error and controller delay. IEEE Trans. Neural Syst. Rehabil. Eng., 19(2):186-192. https://doi.org/10.1109/TNSRE.2010.2100828

[16] Lee SW, Wilson KM, Lock BA, Kamper DG (2011) Subject-specific myoelectric pattern classification of functional hand movements for stroke survivors. IEEE Trans. Neural Syst. Rehabil. Eng., 19(5):558-566. https://doi.org/10.1109/TNSRE.2010.2079334

[17] Bangor A, Kortum P, Miller J (2009) Determining what individual SUS scores mean: Adding an adjective rating scale. J. Usability Stud., 4(3):114-123.

[18] Guo B, Ma Y, Yang J, Wang Z, Zhang X (2020) Lw-CNN-based myoelectric signal recognition and real-time control of robotic arm for upper-limb rehabilitation. Comput. Intell. Neurosci., 2020:8846021. https://doi.org/10.1155/2020/884602

[19] Trigili E, Grazi L, Crea S, Accogli A, Carpaneto J, Micera S, Vitiello N, Panarese A (2019) Detection of movement onset using EMG signals for upper-limb exoskeletons in reaching tasks. J. NeuroEngineering Rehabil., 16:45. https://doi.org/10.1186/s12984-019-0512-1

[20] Zhao D, Ye X, Wang S, Zhang C, Sun S, Zhang X, Cheng R (2025) Upper limb human-exoskeleton system motion state classification based on sEMG: Application of CNN-BiLSTM-attention model. Sci. Rep., 15:18969. https://doi.org/10.1038/s41598-025-02864-5